coatings

Article

Effect of Ultrafast Broadband Nonlinear Optical Responses by Doping Silver into Ti_3C_2 Nanosheets at Visible Spectra

Yabin Shao [1], Chen Chen [2], Qing He [3], Lingling Xiang [1] and Xianjing Lai [1,*]

[1] College of Jia Yang, Zhejiang Shuren University, Shaoxing 312028, China; shao_yabin@163.com (Y.S.); melody.xiang@vip.163.com (L.X.)
[2] College of Information Engineering, East University of Heilongjiang, Harbin 150086, China; rukawa1600@163.com
[3] Collaborative Innovation Center of Steel Technology, University of Science and Technology Beijing, Beijing 100083, China; 123simon@163.com
* Correspondence: laixianjing@163.com

Abstract: Ti_3C_2 nanosheet is a newly discovered two-dimensional (2D) clan. It turns out to have encouraging applications for electromagnetic shielding and energy storage. Here, Ag@ Ti_3C_2 hybrids are precisely synthesized by using the one-step solution processing method. Also, their ultrafast broadband nonlinear optical responses in the visible region are studied systematically through nanosecond open-aperture Z-scan and transient absorption techniques. The mechanism of two-photon absorption (TPA) is disclosed in the visible region (409–532 nm). When the laser energy is low and the wavelength is longer than 400 nm, nonlinear absorption cannot happen. Meanwhile, as the laser energy increases, two photons will be absorbed by the electrons in the valence band and the electrons will jump to the conduction band. The process is named as two-photon absorption which will make the specimen show reverse saturable absorption (RSA) properties. What is more, the ultrafast carrier dynamics of the specimen are studied by using the transient absorption. The result shows that the decay contains two phases: the fast and then the slow one. The two phases first come from electron–phonon and then from phonon–phonon interactions, respectively. The electron transfer and charge carrier trapping processes are further verified by the outcomes of similar measurements on Ag@ Ti_3C_2 hybrids. Besides, the two decay processes increase together with the pump fluence. These results show that Ti_3C_2 nanosheet has potential applications in broadband optical limiter.

Keywords: 2D metamaterial; MXene; optical nonlinear

check for updates

Citation: Shao, Y.; Chen, C.; He, Q.; Xiang, L.; Lai, X. Effect of Ultrafast Broadband Nonlinear Optical Responses by Doping Silver into Ti_3C_2 Nanosheets at Visible Spectra. *Coatings* **2022**, *12*, 189. https://doi.org/10.3390/coatings12020189

Academic Editor: Vera Marinova

Received: 15 January 2022
Accepted: 26 January 2022
Published: 1 February 2022

1. Introduction

With the discovery of graphene, much attention has been placed on two-dimensional (2D) materials to promote the research of modern nonlinear optics owing to their layers of atomic structure, strong light–mater interaction and huge nonlinear optical effect [1]. They have been found to have numerous applications in photonics and optoelectronics [2]. Due to their remarkable optical properties, many 2D materials such as few-layer bismuthene [3], transition metal dichalcogenides (TMD), black phosphorus (BP) [4] and antimonene [5], have promising prospects for mode-locked laser, optical modulator, ultrafast laser generation, photodetectors, etc. [6]. On the other hand, some inherent flaws of them remain a challenge for further applications. For example, graphene has a direct bandgap and BP exhibits unstable characters in the air [7,8]. As a result, the final application of promising 2D nonlinear optical (NLO) materials still has a long way to go. As the latest branch of 2D materials, MXenes have captured much attention among scholars due to their fine conductivity, large elastic moduli, great electric capacity, tunable bandgap, and more admirable optical transparency [9–13]. So far, more than 30 types of different MXenes have been reported, showing the growing members of the MXene family [14]. Moreover, the abundant nature of chemistries and electronic band structure enrich the application base on MXenes from energy storage and biomedicine to nonlinear photonics and nuclear waste management [15,16]. Typically, to achieve the application-oriented demands for MXenes, various modification techniques have been performed to obtain the same desired functionalities as the previous studies on colloidal solutions of nanoparticles (NPs) hybridized by graphene, TMDs, etc. [17]. Furthermore, the breakthrough of hybridizing NPs for NLO application has emerged in the past several years in terms of their defect states, surface control, and excellent plasmonic properties [18–20]. Ti3Ce, initially synthesized by Gogotsi et al. in 2011 [21], is the first member of the MXene family. It has gained widespread use in NLO components [14], optoelectronic devices [22] and electromagnetic applications [23] owing to its unique features of atomic structures. While, in visible light region, silver (Ag) can act as an excellent dopant accompanied by functional advantages of increasing the excited absorption cross-section and promoting absorption in the excited state. Silver nanoparticles, though they oxidize rapidly in the air, are favored for their bactericidal properties. The method of not being oxidized in oxygen is still being investigated. As an intriguing semiconductor noble metal hybrid, the Ag@ Ti_3C_2 nanostructure had been successfully synthesized by Satheeshkumar et al. It shows the encouraging Surface-Enhanced Raman Scattering (SERS) [24] and surface plasmon resonance (SPR) properties [25]. The effect of SPR arising from the Ag nanoparticles plays a vital role in the proposed structure in other works [26–28]. With noble metal inducing SPR, the NLO responses can be enhanced significantly and the outperformance can happen in pulsed lasing [29].

Here, to acquire the functionalization of Ti_3C_2 for NLO applications, we have built a hybridized system of Ti_3C_2 and Ag NPs with the sole step without an external reducing agent or surfactant as illustrated in the abstract above which is environmentally benign [24]. Ultrafast carrier dynamic and nonlinear absorption of Ag@ Ti_3C_2 hybrids in the visible spectral region are researched. It is significant to reveal the nonlinear absorption properties of that at a broadband wavelength range from 409 to 532 nm by nanosecond Z scan measurement. Besides, the character of optical limiter is studied in detail. The carrier dynamics of this hybrid are investigated with femtosecond transient absorption experiments which can be used to study the decaying channels at various energy levels with multiple probe wavelengths.

2. Specimen and Experiments

The Ti_3C_2 used in this work is manufactured by selectively etching Al from the MAX precursors Ti_3AlC_2Tx. Synthesizing details can be found elsewhere [30]. The Ag@Ti_3C_2 hybrids are made ready by mingling the Ti_3C_2 nanosheet dispersion and $AgNO_3$ solution. They are shown in Figure 1. First, we re-dispersed 3 mL of original Ti_3C_2 nanosheet colloidal solution (1 mg/mL) in 30 mL of $AgNO_3$ solution (1 mg/mL) and sonicated the mixture for 30 min. Then, we centrifuged the obtained colloidal solution of hybrid nanocomposites of Ag@ Ti_3C_2 hybrids at 12,000 rpm for 20 min and re-dispersed in 30 mL deionized water.

By scanning electron microscopy (SEM, ZEISS ULTRA 55, Oberkochen, Germany), we observed the Microstructure features of Ag@ Ti_3C_2 hybrids and Ti_3C_2. Furthermore, the monolayered structures are displayed by transmission electron microscopy (TEM, (FEI Tecnai G2 F20, Hillsboro, OR, USA), and the element mapping was captured by STEM-EDX mapping. At room temperature, we surveyed the absorbance spectra of Ti_3C_2 nanosheet with a UV-vis spectrometer ((TU-1901, Persee, Auburn, CA, USA).

With 6 ns Q-switched Nd: YAG nanosecond pulse laser ((Surelite II, Continuum, San Jose, CA, USA), we applied the approaches of open-aperture Z-scan to detect the NLO absorption features of Ag@ Ti_3C_2 hybrids solutions. To evade the thermally induced nonlinear scattering, the laser repetition rate was set at 5 Hz. To obtain the lasers (410–700 nm), an optical parametric oscillator (OPO) was employed [31]. The laser beam (ω_0 = 200 μm) was focused through a lens (f = 20 cm) onto a quartz cuvette (2 mm) full of Ag@ Ti_3C_2. While the specimen changes its position on the translation stage (TSA200, Zolix, Beijing, China), the transmittance signals are detected precisely, with the Z-scan signals gathered by an energy detector (J-10MB-LE, Coherent, Santa Clara, CA, USA) and recorded through an energy meter (EPM2000, Coherent, Santa Clara, CA, USA). The ultrafast carrier dynamics were revealed by femtosecond transient absorption spectroscopy measurements. The laser pulse (~35 fs, 800 nm and 1 kHz) is originally created through Ti: sapphire regenerative amplifier ((Astrella, Coherent, Santa Clara, CA, USA). What is more, a BBO crystal is employed to double the photon energy to 400 nm. A sapphire plate is adopted to get white-light continuum (420 to 750 nm) as a probe beam which is concentrated through a quartz cuvette (2 mm) filled with Ag@ Ti_3C_2 aqueous solution. The intensity of both transmitted probe and reference beams were detected by two spectrometers (Avantes-950F, Avantes, Apeldoorn, the Netherlands), respectively, after the specimen was delayed relatively by a delay line (TSA00, Zolix, Beijing, China). All the signals were input to a computer synchronously. Through a standard specimen, pump and probe beams are overlapped spatially. By using optical Kerr signal from the SiO_2 substrate, we affirmed the group-velocity dispersion of the white-light continuum [32].

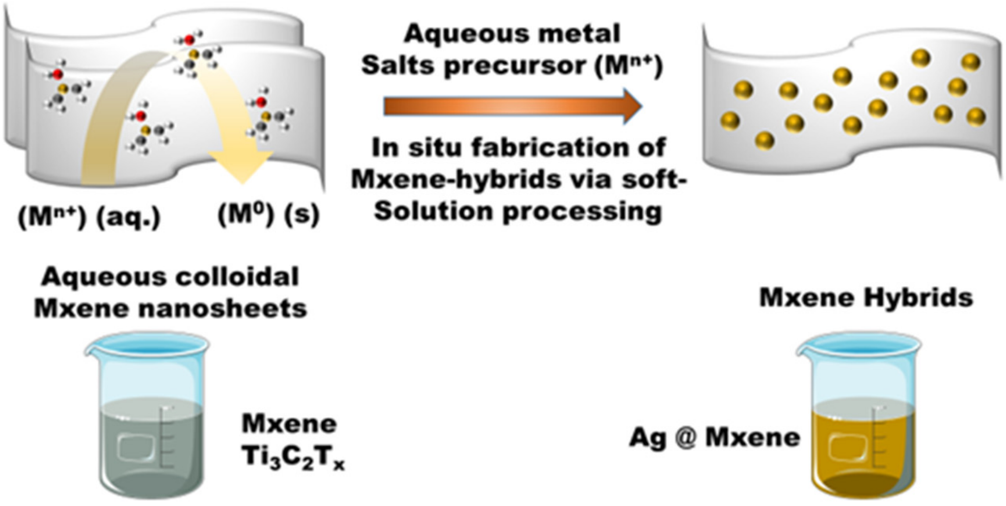

Figure 1. The structural schematic of the proposed hybrid metal–graphene material, and the parameters of the proposed unit structure.

3. Result and Discussion

The morphologic structures of Ag@ Ti_3C_2 and Ti_3C_2 are shown in Figure 2. The TEM images and HRTEM images EDX analysis pictures of Ti_3C_2 are presented in Figure 2a,b, ~1 µm monolayered Ti_3C_2 nanosheet can be observed and Ti, C, and O elements are displayed in Figure 2a. Aside from the inherent Ti–C bond, the Ti_3C_2 nanosheets are predominantly oxygen-terminated. A finer structure is shown in Figure 2b. Through applying a mixture of AgNO3 and Ti_3C_2 solution during synthesis of the Ag@ Ti_3C_2 rather than pure Ag, situ Ag doping of the Ti_3C_2 structure is obtained without compromising the accordion-like Ti_3C_2 structure. Plenty of Ag nanoparticles was dispersed uniformly in Ti_3C_2, which can be observed in Figure 2c. Meanwhile, the observed structure, which can be seen in the X-ray powder diffraction (XRD, Seifert-FPM, Freiberg, Germany) pattern in Figure 3a, is consistent with morphological results. In order to further illustrate the microscopic results of the material, the selected area of the yellow square in Figure 2a,e is enlarged to obtain Figure 2b,d. The cross-section of layered Ti_3C_2 structure in Figure 2d and the distributed Ag on Ti_3C_2 flakes are shown. The SPR effect dominates by the particle size, gap distance among adjacent AgNPs [26], resulting in the hybridization of surface plasmon resonance [33] and gap plasmon resonance [27]. In this work, the average particle size of AgNPs was ~6–10 nm. Figure 2e presents the TEM micrographs, respectively. The experiment results proved that Ag nanoparticles (the bright particles) are inlaid into Ti_3C_2 nanosheet with one accord. Furthermore, in order to determine the composition of the obtained Ag@ Ti_3C_2, Ti, C, O, and Ag elements are shown in EDX analysis in Figure 2f.

In brief, all the results presented below show that the doping Ag is uniformly distributed throughout the entire Ti_3C_2 structure.

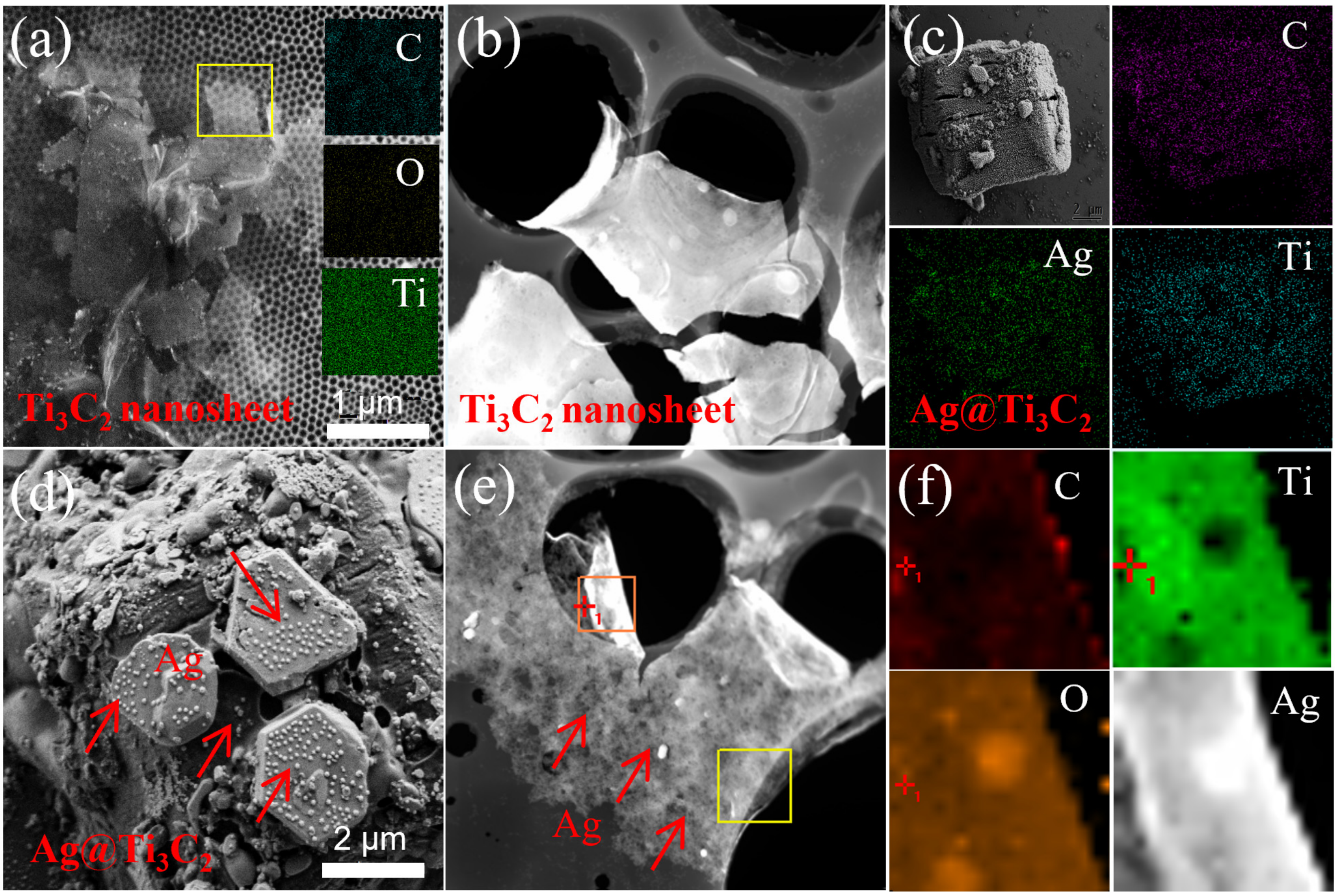

Figure 2. (**a**,**b**) TEM and EDS image of Ti_3C_2 and (**c**) Ag@Ti_3C_2. (**d**) TEM image of conventional Ag@Ti_3C_2 (**e**) The high-resolution TEM image (**f**) STEM-EDX mapping of Ag@Ti_3C_2.

The phase transitions of hybridization researched by XRD are displayed in Figure 3a. Two peaks of Ag diffraction and Ti_3C_2 that are shifted to a much lower angle compared with that of the specimen revealed the expansion of the interlayer distance. In Figure 3b, the Ag@ Ti_3C_2 shows an absorption peak at ~436 nm, which is due to the formation of Ag nanoparticles [24]. As shown in Figure 3b, two absorption peaks are observed at 245 and 325 nm, respectively. These results are under expectation.

As shown in Figure 3b, we find the high absorption in the UV region ranging from 225 to 375 nm as a result of the band-gap energy of the oxidized MXene, which is also predicted by previous theoretical calculations [34,35].

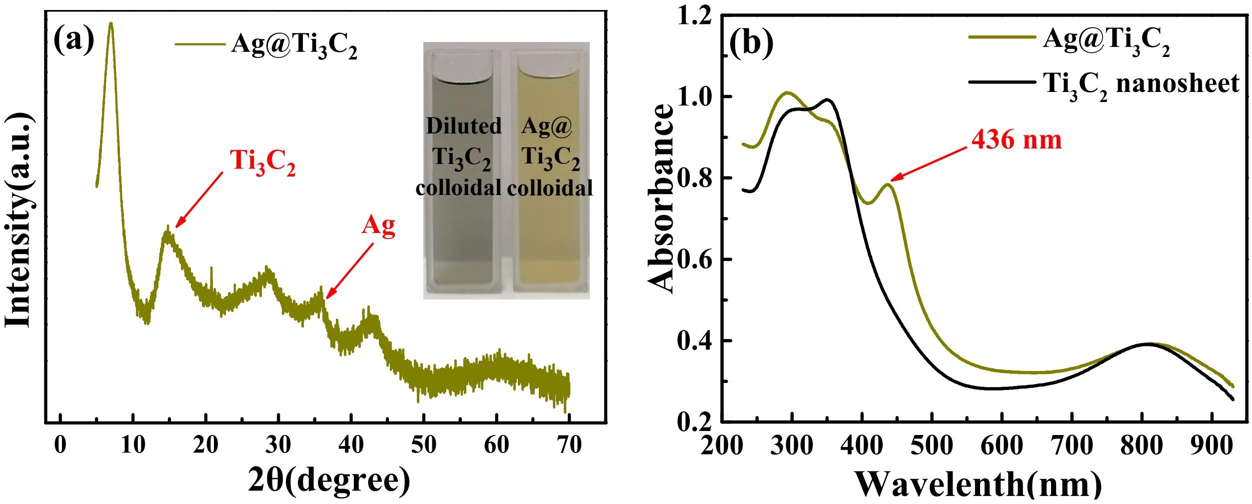

Figure 3. (**a**) XRD pattern of Ag@Ti_3C_2, (**b**) linear absorption spectra of Ag@Ti_3C_2 and Ti_3C_2 nanosheets.

Open aperture Z-scan data of Ti_3C_2 dispersions are shown in Figure 4a–d. It is obtained at four laser wavelengths of 409, 436, 500, and 532 nm. Specially, in Figure 4b, at the resonant wavelength of 436 nm, the measurement is applied to study the optical nonlinearity of the Ag@Ti_3C_2 nanosheet under the laser pulse energy of 0.11, 0.36 and 0.64 GW/cm^2. When the specimen reaches the focal plane (z = 0), we notice the formation of a shallower valley, which indicates that reverse saturable absorption (RSA) arises. A greater enhancement of optical nonlinearity than that of the Ti_3C_2 nanosheet is observed in our previous work [30]. The experiment results under the other three wavelengths also exhibit RSA properties. In Figure 4a, when incident pulsed laser energy is 0.11 and 0.36 GW/cm^2, the normalized transmittances of specimens remain unchanged and no signals are observed. When the pulsed laser energy reaches 0.64 GW/cm^2, the transmittances decrease correspondingly. As shown in Figure 4b,c, when the energy is from 0.11 to 0.64 GW/cm^2, a deeper valley appears. In Figure 4d, as RSA is shown under the energy of 0.36–0.64 GW/cm^2, no experimental signal is observed under 0.11 GW/cm^2. The findings of the experiments in Figure 4a,d disclose that the result of RSA is not clear at fewer inputs of energy. Accordingly, we raised the input energy to carry out the following experiments. In short, broad-band RSA appears on Ag@Ti_3C_2 nanosheet, which proves that it is potentially applicable to optical limiting devices.

The absorbance spectra in Figure 3b show that the one-photon absorption effect only takes place when the wavelength amounts to no more than 400 nm. Thus, the physical process of RSA can be concluded as follows. When laser energy is low, nonlinear absorption cannot happen. However, with the laser energy increased, two photons will be absorbed by the electrons in the valence band and the latter will jump to the conduction band. To put it another way, two-photon absorption would occur and make the specimen display RSA [36].

Electron transfer between Ti_3C_2 and Ag atoms will arise when Ag nanoparticles are doped into it. From Figure 5b, we should notice TA spectra of the Ag@Ti_3C_2 and the occurrence of the excited state absorption. The strengthened absorption, compared with pure Ti_3C_2, may arise from the absorption of photo-induced surface plasmon in Ag nanoparticles [31].

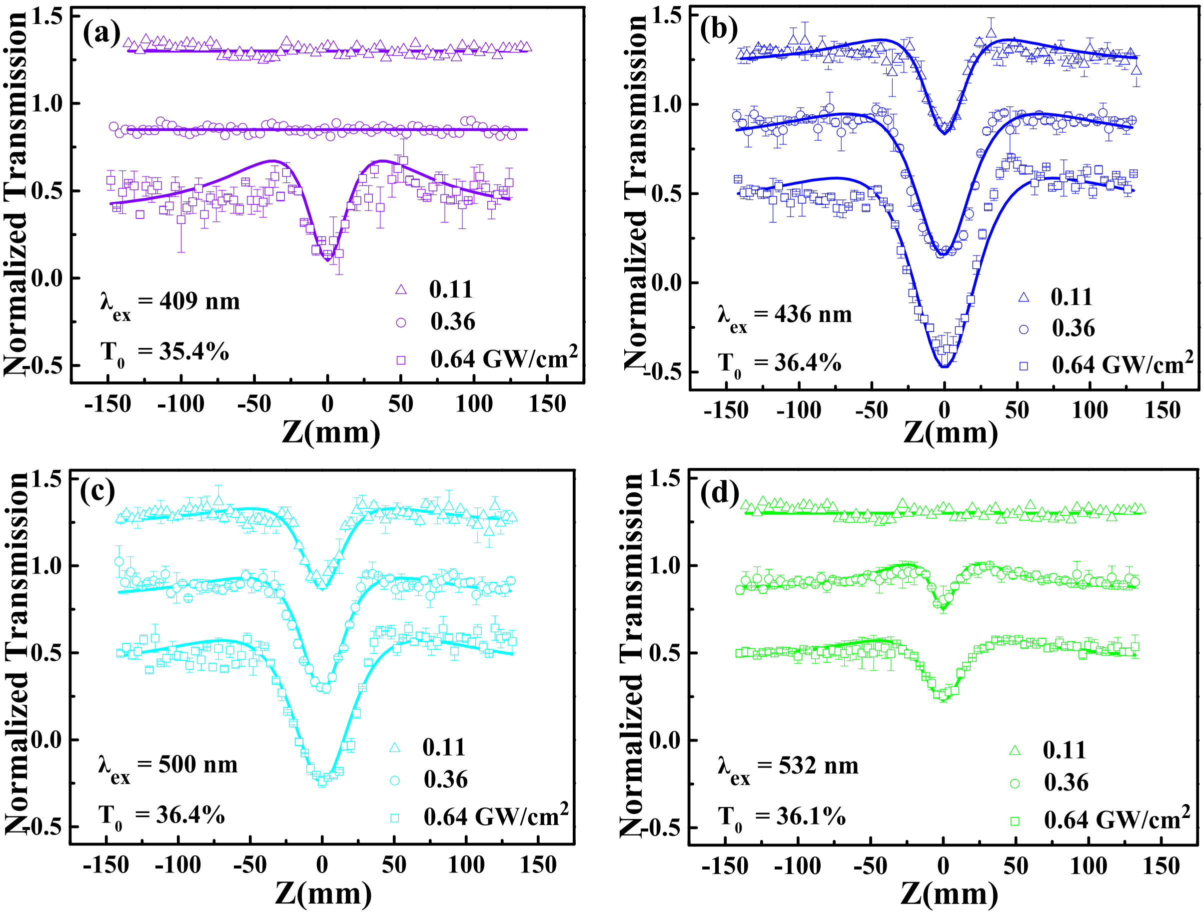

Figure 4. Normalized transmission of Ag@Ti_3C_2 dispersion for open aperture Z-scan at the wavelength of (**a**) 409 nm, (**c**) 500 nm, and (**d**) 532 nm. (**b**) Ag@Ti_3C_2 and Ti_3C_2 nanosheet dispersion open aperture Z-scan data for comparison.

Based on the above analysis, we combine the SA and the RSA to achieve the total absorption coefficient as follows [37]:

$$\alpha(I) = \frac{\alpha_0}{1 + (I/I_s)} + \beta I \tag{1}$$

Here in Equation (1), α_0 signifies the linear absorption coefficient, I the pulse laser intensity, and I_s the saturable intensity. To suppress interference of the solvents in the nonlinear effect, we apply the Z-scan measurement to the solvents within the same parameters. The normalized transmission of the open aperture Z-scan is illustrated as below [38]:

$$T = \sum_{m=0}^{\infty} \frac{[-q_0(z)]^m}{(m+1)^{\frac{3}{2}}} \approx 1 - \frac{\beta I_0 L_{eff}}{2\sqrt{2}(1 + \frac{z^2}{z_0^2})} \tag{2}$$

Here in Equation (2), β signifies the nonlinear absorption coefficient; I_0 the peak intensity at the focus; L the distance that the light passes through the specimen; L_{eff} the effective interaction length which could be elaborated as $L_{eff} = (1 - e^{-\alpha}{}_0{}^{1})/\alpha_0$; z the displacement of the specimen along the stage from the focal point ($z = 0$); and z_0 the Rayleigh diffraction length.

In Figure 4, we use Equations (1) and (2) to achieve the theoretical fit and the nonlinear absorption coefficient β, the former is drawn in solid lines and latter listed in Table 1. The conclusion is that the TPA coefficients are obtained along with each wavelength increase, and laser irradiance increases synchronously. These findings are advantageous when they are used to limit the optical intensity to protect human eyes as well as optical devices.

Table 1. Nonlinear optical parameters of the Ti_3C_2 nanosheet.

λ (nm)	**I_0 (10^{-2} GW/cm^2)**	**β (10^{-9} cm/mW)**
409	0.74	-
	1.10	-
	1.40	1.80 ± 0.11
500	0.74	0.91 ± 0.06
	1.10	1.12 ± 0.09
	1.40	1.81 ± 0.12
436	0.74	1.03 ± 0.08
	1.10	1.32 ± 0.10
	1.40	1.93 ± 0.13
532	0.74	-
	1.10	0.41 ± 0.05
	1.40	0.78 ± 0.06

We take the measure of broadband transient absorption to study the ultrafast carrier dynamics of Ag@Ti_3C_2 and Ti_3C_2 nanosheet. To find the different carrier dynamics between Ag@Ti_3C_2 and Ti_3C_2 nanosheet, the broadband TA under the 400 nm pump is set at the constant pump fluence of 6.4×10^3 mW/cm^2. In Figure 6a,c, the TA spectra with multiple probe beams (450 to 600 nm) of Ag@Ti_3C_2 and Ti_3C_2 nanosheet are demonstrated by a 2D map comprising TA signals in a temporal and spectral sense. Obviously, a brighter zone is given in Figure 5a than that in Figure 5b, which implies that enhanced signals emerged according to Ag nanoparticles in the Ti_3C_2 nanosheet. The plasmonic effects, that of SPR is arising from the Ag nanoparticles [27]. As shown in Figure 5b,d, five differential horizontal cuts through the 2D map illustrate the absorption spectra that vary with distinct delay time. In Figure 5b, a positive absorption in Ag@Ti_3C_2 proves that the excited state absorption (ESA) occurs in the whole spectral region. Furthermore, the amplitude of the Transient Absorption (TA) spectrum descends while the delay time ascends, which could be ascribed to the carrier relaxation. We adopt the curve of 0 ps delay time (black) as a reference signal before the Ti_3C_2 nanosheet being excited. The transition process between occupied and unoccupied states results in photo-induced absorption that leads to the peak of Ag@Ti_3C_2 at the wavelength of 495 nm, which is the mutual proof of the observations of RSA in Z-scan experiment [39–41]. It costs the TA signal ~50 ps to relax from the peak to zero in the full waveband. In Figure 5d, the semblable behavior is shown in Ti_3C_2 nanosheet, and in ~25 ps, the TA signal relaxes to zero. It is quite interesting that Ag@Ti_3C_2 exhibits enhanced nonlinear optical in contrast with that in pure Ti_3C_2 nanosheet.

In the TA experiment, we used a 400 nm (~3.1 eV) pump light laser whose energy is stronger than the energy bandgap of Ti_3C_2 nanosheets (~2.04 eV). In general, after the specimen is pumped by incident pulses, electrons in the valence band (VB) will be excited and jumped onto the conduction band (CB) through the Franck–Condon transition in several femtoseconds. Meanwhile, the holes will remain in the valence band [42]. Afterwards, carriers that have been excited by photons will be immediately transformed into hot carriers with Fermi–Dirac distribution. Consequently, the hot carriers will follow different relaxation processes through electron–electron and electron–phonon scatterings, which produce the electrons to the conduction band minimum in several picoseconds. In the end, the electrons will cool down, and in tens of picoseconds, it will relax back to VB and reunite with the remaining holes.

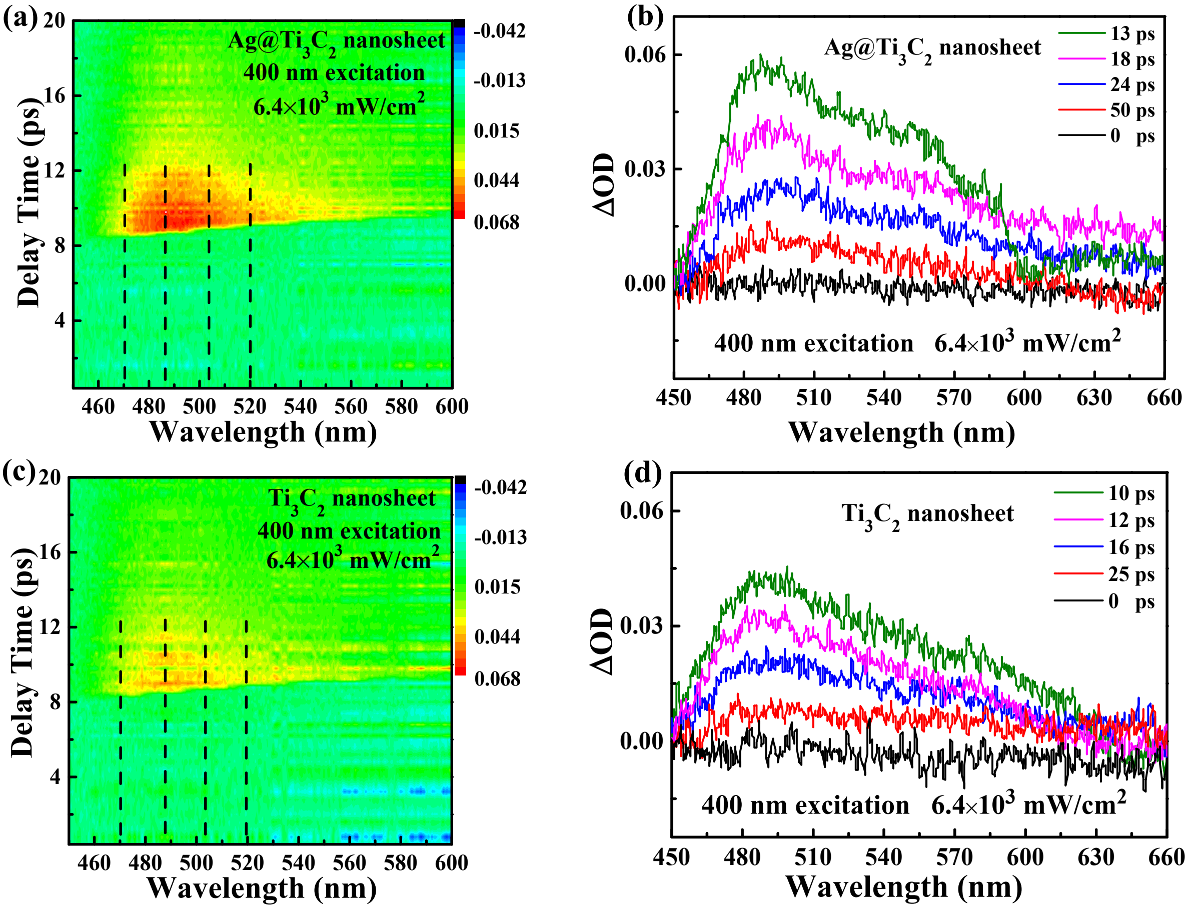

Figure 5. (**a**,**c**) Two-dimensional (2D) mapping of transient absorption (TA) spectra for Ag@Ti_3C_2 and Ti_3C_2 nanosheet pumped at 400 nm with a fluence of 6.4×10^3 mW/cm^2. (**b**,**d**) Time and wavelength resolved transient absorption data of Ag@Ti_3C_2 and Ti_3C_2 nanosheet.

To examine the carrier dynamics at multiple wavelengths, we chart Figure 6a,b to illustrate the normalized dynamics curves at the wavelength of 470, 485, 500 and 525 nm, among which Figure 6a explains the optical transmission responses of Ag@Ti_3C_2 that include a fast decay component and a slow one. We attribute the two components to their corresponding decay processes. After excitation, the fast decay component comes first and Coulomb-induced hot carriers will be trapped from the core state to the surface state. Their spare energy will be released via optical phonon scattering (~4.5 ps). Then comes the slow decay component and the cooled carriers will pass through nonradiative transition to the ground state within ~43 ps [20,43]. The two different decay components are demonstrated by Equation (3), the biexponential decay function as shown below [44]:

$$\frac{\Delta T}{T} = A_1 \exp(-\frac{t}{\tau_1}) + A_2 \exp(-\frac{t}{\tau_2}) \tag{3}$$

where A_1, A_2 are the amplitudes of each decay components. τ_1 and τ_2 refer to two parameters, describing fast and slow decay lifetimes.

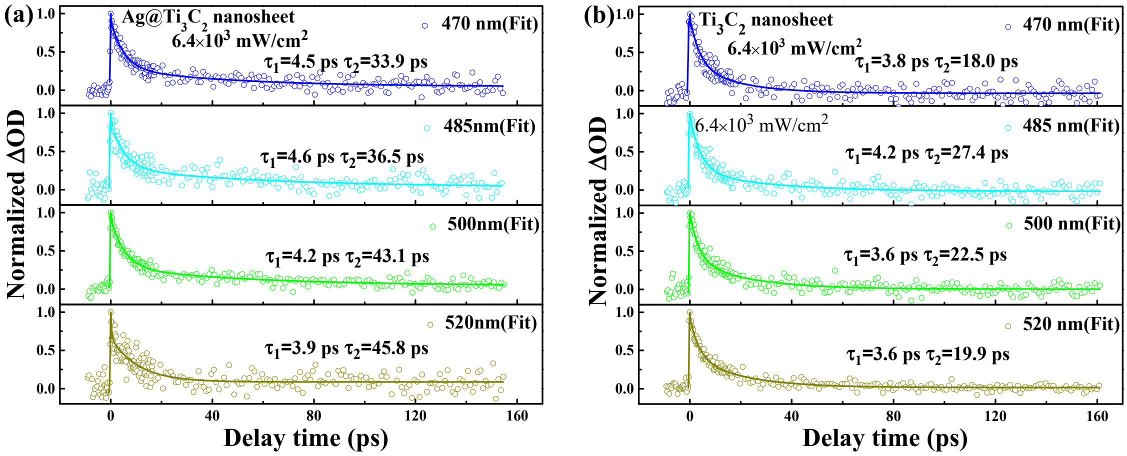

Figure 6. Carrier dynamics (at 400 nm pump) curves for (**a**) Ag@Ti$_3$C$_2$ and (**b**) Ti$_3$C$_2$ nanosheet at different probe wavelengths of 470, 485, 500, and 520 nm, respectively (the data points are experimental data while the solid lines are the curves of theoretical fits) with pump fluence fixed at 6.4×10^3 mW/cm^2.

As shown in Figure 6, we use Equation (3) to obtain the theoretical fits of the fast relaxation components (τ_1) and slow relaxation components (τ_2) and list them in Table 2.

Table 2. Carrier dynamics parameters of the Ti$_3$C$_2$ nanosheet.

Samples	λ (nm)	τ_1 (ps)	τ_2 (ps)
Ag@Ti$_3$C$_2$	470	4.5	33.9
	485	4.6	36.5
	500	4.2	43.1
	520	3.9	45.8
Ti$_3$C$_2$ nanosheet	470	3.8	18.0
	485	3.2	27.4
	500	4.6	22.5
	520	4.6	19.9

It is argued that electrons on the lower energy states tend to be probed more readily than those on higher energy states. An analogous phenomenon was observed in graphite [45]. As Ag has tremendous states density, the excited electrons in the CB of Ti$_3$C$_2$ will jump to the d band of Ag atoms before the bleaching effect of VB vanishes [46]. Thus, the process prolongs the lifetime of excited electrons which will lead to a stronger RSA response. Afterwards, the electrons in the d band of Ag atoms will jump to the corresponding excited state of functional teams which will absorb the laser energy and jump to the higher energy level. Hence, the enhanced RSA is induced. Ornamented with Ag nanoparticles, the excited carriers from the CB of Ti$_3$C$_2$ will first move to the sp band of the particles and then turn back to VB of Ag@Ti$_3$C$_2$. This process will happen in a longer lifetime (50 ps) than the direct relaxation in pure Ti$_3$C$_2$ nanosheet, which leads to the elevation of RSA, a similar phenomenon found in graphene [47].

4. Conclusions

The NLO absorption properties of Ti$_3$C$_2$ nanosheet is systematically researched through an OA z-scan technique to reach the conclusion that at broadband visible range (409–532 nm), Ti$_3$C$_2$ nanosheet exhibits RSA properties which are resulting mainly from TPA. What is more, we adopt femtosecond transient absorption spectroscopy to study ultrafast dynamics of the specimen to find that its relaxation contains a fast decay component (~4 ps), resulting from electron –phonon interaction, and a slow one (~12 ps), from phonon–phonon interaction. Besides, the two decay times increase with pump fluence. The experiment confirms that Ti_3C_2 nanosheets can be used in ultrafast optoelectronics and optical limiters.

Author Contributions: Data curation, C.C.; Funding acquisition, X.L.; Investigation, Y.S.; Resources, Q.H.; Writing—review and editing, L.X. All authors have read and agreed to the published version of the manuscript.

Funding: The article was supported by the following funds, Natural Science Foundation of Heilongjiang Province (Grant No. LH2021A019), East University of Heilongjiang Scientific Research Fund (Grant Nos. HDFHX210110, 210111, HDFKYTD202105), Scientific research fund of Zhejiang Shuren University(Grant No. 2021R037).

Institutional Review Board Statement: Not applicable.

Informed Consent Statement: Not applicable.

Data Availability Statement: Data sharing is not applicable to this article.

Conflicts of Interest: The authors declare no conflict of interest.

References

1. You, J.W.; Bongu, S.R.; Bao, Q.; Panoiu, N.C. Nonlinear optical properties and applications of 2D materials: Theoretical and experimental aspects. *Nanophotonics* **2019**, *8*, 63–97. [CrossRef]
2. Tan, T.; Jiang, X.; Wang, C.; Yao, B.; Zhang, H. 2D Material Optoelectronics for Information Functional Device Applications: Status and Challenges. *Adv. Sci.* **2020**, *7*, 2000058–2000083. [CrossRef] [PubMed]
3. Lu, L.; Liang, Z.; Wu, L.; Chen, Y.; Song, Y.; Dhanabalan, S.C.; Ponraj, J.S.; Dong, B.; Xiang, Y.; Xing, F.; et al. Few-layer Bismuthene: Sonochemical Exfoliation, Nonlinear Optics and Applications for Ultrafast Photonics with Enhanced Stability (Laser Photonics Rev. 12(1)/2018). *Laser Photonics Rev.* **2018**, *12*, 1870012. [CrossRef]
4. Jiang, T.; Yin, K.; Wang, C.; You, J.; Ouyang, H.; Miao, R.; Zhang, C.; Wei, K.; Li, H.; Chen, H.; et al. Ultrafast fiber lasers mode-locked by two-dimensional materials: Review and prospect. *Photonics Res.* **2020**, *8*, 78–90. [CrossRef]
5. Lu, L.; Tang, X.; Cao, R.; Wu, L.; Li, Z.; Jing, G.; Dong, B.; Lu, S.; Li, Y.; Xiang, Y.; et al. Quantum Dots: Broadband Nonlinear Optical Response in Few-Layer Antimonene and Antimonene Quantum Dots: A Promising Optical Kerr Media with Enhanced Stability (Advanced Optical Materials 17/2017). *Adv. Opt. Mater.* **2017**, *5*, 1700301. [CrossRef]
6. Autere, A.; Jussila, H.; Dai, Y.; Wang, Y.; Lipsanen, H.; Sun, Z. Nonlinear Optics with 2D Layered Materials. *Adv. Mater.* **2018**, *30*, 1705963. [CrossRef]
7. Zhou, Q.; Chen, Q.; Tong, Y.; Wang, J. Light-Induced Ambient Degradation of Few-Layer Black Phosphorus: Mechanism and Protection. *Angew. Chem. Int. Ed.* **2016**, *55*, 11437–11441. [CrossRef]
8. Currie, M.; Caldwell, J.D.; Bezares, F.J.; Robinson, J.; Anderson, T.; Chun, H.; Tadjer, M. Quantifying pulsed laser induced damage to graphene. *Appl. Phys. Lett.* **2011**, *99*, 211909. [CrossRef]
9. Keller, U. Recent developments in compact ultrafast lasers. *Nature* **2003**, *424*, 831–838. [CrossRef]
10. Mashtalir, O.; Naguib, M.; Mochalin, V.N.; Dall'Agnese, Y.; Heon, M.; Barsoum, M.W.; Gogotsi, Y. Intercalation and delamination of layered carbides and carbonitrides. *Nat. Commun.* **2013**, *4*, 1716. [CrossRef]
11. Lukatskaya, M.R.; Mashtalir, O.; Ren, C.E.; Dall'Agnese, Y.; Rozier, P.; Taberna, P.L.; Naguib, M.; Simon, P.; Barsoum, M.W.; Gogotsi, Y. Cation intercalation and high volumetric capacitance of two-dimensional titanium carbide. *Science* **2013**, *341*, 1502–1505. [CrossRef]
12. Shahzad, F.; Alhabeb, M.; Hatter, C.B.; Anasori, B.; Hong, S.M.; Koo, C.M.; Gogotsi, Y. Electromagnetic interference shielding with 2D transition metal carbides (MXenes). *Science* **2016**, *353*, 1137–1140. [CrossRef]
13. Peng, Q.; Guo, J.; Zhang, Q.; Xiang, J.; Liu, B.; Zhou, A.; Liu, R.; Tian, Y. Unique lead adsorption behavior of activated hydroxyl group in two-dimensional titanium carbide. *J. Am. Chem. Soc.* **2014**, *136*, 4113–4116. [CrossRef]
14. Gogotsi, Y.; Anasori, B. The Rise of MXenes. *ACS Nano* **2019**, *13*, 8491–8494. [CrossRef]
15. Anasori, B.; Lukatskaya, M.R.; Gogotsi, Y. 2D metal carbides and nitrides (MXenes) for energy storage. *Nat. Rev. Mater.* **2017**, *2*, 16098–18114. [CrossRef]
16. Jiang, X.T.; Zhang, L.J.; Liu, S.X.; Zhang, Y.Y.; He, Z.L.; Li, W.J.; Zhang, F.; Shi, Y.H.; Lu, W.; Li, Y.; et al. Ultrathin Metal-Organic Framework: An Emerging Broadband Nonlinear Optical Material for Ultrafast Photonics. *Adv. Opt. Mater.* **2018**, *6*. [CrossRef]
17. Kim, I.Y.; Jo, Y.K.; Lee, J.M.; Wang, L.; Hwang, S.-J. Unique Advantages of Exfoliated 2D Nanosheets for Tailoring the Functionalities of Nanocomposites. *J. Phys. Chem. Lett.* **2014**, *5*, 4149–4161. [CrossRef]
18. Biswas, S.; Kole, A.K.; Tiwary, C.S.; Kumbhakar, P. Enhanced nonlinear optical properties of graphene oxide–silver nanocomposites measured by Z-scan technique. *RSC Adv.* **2016**, *6*, 10319–10325. [CrossRef]
19. Li, Z.; Dong, N.; Cheng, C.; Xu, L.; Chen, M.; Wang, J.; Chen, F. Enhanced nonlinear optical response of graphene by silver-based nanoparticle modification for pulsed lasing. *Opt. Mater. Express* **2018**, *8*, 1368–1377. [CrossRef]

20. Yan, X.; Wu, X.; Fang, Y.; Sun, W.; Yao, C.; Wang, Y.; Zhang, X.; Song, Y. Effect of silver doping on ultrafast broadband nonlinear optical responses in polycrystalline Ag-doped InSe nanofilms at near-infrared. *RSC Adv.* **2020**, *10*, 2959–2966. [CrossRef]
21. Naguib, M.; Kurtoglu, M.; Presser, V.; Lu, J.; Niu, J.; Heon, M.; Hultman, L.; Gogotsi, Y.; Barsoum, M.W. Two-Dimensional Nanocrystals Produced by Exfoliation of Ti_3AlC_2. *Adv. Mater.* **2011**, *23*, 4248–4253. [CrossRef]
22. Wang, Y.; Xu, Y.; Hu, M.; Ling, H.; Zhu, X. MXenes: Focus on optical and electronic properties and corresponding applications. *Nanophotonics* **2020**, *9*, 1601. [CrossRef]
23. Jiang, X.; Kuklin, A.V.; Baev, A.; Ge, Y.; Ågren, H.; Zhang, H.; Prasad, P.N. Two-dimensional MXenes: From morphological to optical, electric, and magnetic properties and applications. *Phys. Rep.* **2020**, *848*, 1–58. [CrossRef]
24. Satheeshkumar, E.; Makaryan, T.; Melikyan, A.; Minassian, H.; Gogotsi, Y.; Yoshimura, M. One-step Solution Processing of Ag, Au and Pd@MXene Hybrids for SERS. *Sci. Rep.* **2016**, *6*, 32049–32055. [CrossRef]
25. Yang, W.; Zhang, L.; Hu, Y.; Zhong, Y.; Wu, H.B.; Lou, X.W. Microwave-Assisted Synthesis of Porous Ag_2S–Ag Hybrid Nanotubes with High Visible-Light Photocatalytic Activity. *Angew. Chem. Int. Ed.* **2012**, *51*, 11501–11504. [CrossRef]
26. Chau, Y.-F.; Yeh, H.-H. A comparative study of solid-silver and silver-shell nanodimers on surface plasmon resonances. *J. Nanoparticle Res.* **2011**, *13*, 637–644. [CrossRef]
27. Chou Chao, C.-T.; Chou Chau, Y.-F.; Huang, H.J.; Kumara, N.T.R.N.; Kooh, M.R.R.; Lim, C.M.; Chiang, H.-P. Highly Sensitive and Tunable Plasmonic Sensor Based on a Nanoring Resonator with Silver Nanorods. *Nanomaterials* **2020**, *10*, 1399. [CrossRef]
28. Chou Chau, Y.-F.; Chou Chao, C.-T.; Rao, J.-Y.; Chiang, H.-P.; Lim, C.M.; Lim, R.C.; Voo, N.Y. Tunable Optical Performances on a Periodic Array of Plasmonic Bowtie Nanoantennas with Hollow Cavities. *Nanoscale Res. Lett.* **2016**, *11*, 411. [CrossRef]
29. Nie, W.J.; Zhang, Y.X.; Yu, H.H.; Li, R.; He, R.Y.; Dong, N.N.; Wang, J.; Hübner, R.; Böttger, R.; Zhou, S.Q.; et al. Plasmonic nanoparticles embedded in single crystals synthesized by gold ion implantation for enhanced optical nonlinearity and efficient Q-switched lasing. *Nanoscale* **2018**, *10*, 4228–4236. [CrossRef]
30. Shao, Y.; Chen, C.; He, Q.; Wu, W.; Gao, Y. Broadband Visible Nonlinear Absorption and Ultrafast Dynamics of the Ti_3C_2 Nanosheet. *Nanomaterials* **2020**, *10*, 2544. [CrossRef]
31. Shao, Y.; Chen, C.; Han, J.; Kong, D.; Gao, Y. Wavelength-dependent nonlinear absorption and ultrafast dynamics process of WS_2. *OSA Contin.* **2019**, *2*, 2755–2763. [CrossRef]
32. Wu, W.; Zhou, Y.; Wang, J.; Shao, Y.; Wang, Y. The pump fluence and wavelength-dependent ultrafast carrier dynamics and optical nonlinear absorption in black phosphorus nanosheets. *Nanophotonics* **2020**, *9*, 2033–2043. [CrossRef]
33. Chou Chau, Y.-F.; Ming, T.Y.; Chou Chao, C.-T.; Thotagamuge, R.; Kooh, M.R.R.; Huang, H.J.; Lim, C.M.; Chiang, H.-P. Significantly enhanced coupling effect and gap plasmon resonance in a MIM-cavity based sensing structure. *Sci. Rep.* **2021**, *11*, 18515. [CrossRef] [PubMed]
34. Naguib, M.; Gogotsi, Y. Synthesis of two-dimensional materials by selective extraction. *Acc. Chem. Res.* **2015**, *48*, 128–135. [CrossRef]
35. Hu, Q.; Sun, D.; Wu, Q.; Wang, H.; Wang, L.; Liu, B.; Zhou, A.; He, J. MXene: A new family of promising hydrogen storage medium. *J. Phys. Chem. A* **2013**, *117*, 14253–14260. [CrossRef]
36. Wang, G.; Bennett, D.; Zhang, C.; Coileain, C.O.; Liang, M.; Mcevoy, N.; Wang, J.J.; Wang, J.; Wang, K.; Nicolosi, V. Two-Photon Absorption in Monolayer MXenes. *Adv. Opt. Mater.* **2020**, *8*, 1902021–1902029. [CrossRef]
37. Gao, Y.; Zhang, X.; Li, Y.; Liu, H.; Wang, Y.; Chang, Q.; Jiao, W.; Song, Y. Saturable absorption and reverse saturable absorption in platinum nanoparticles. *Opt. Commun.* **2005**, *251*, 429–433. [CrossRef]
38. Sheik-Bahae, M.; Said, A.A.; Wei, T.; Hagan, D.J.; Stryland, E.W.V. Sensitive measurement of optical nonlinearities using a single beam. *IEEE J. Quantum Electron.* **1990**, *26*, 760–769. [CrossRef]
39. Wang, J.; Ding, T.; Wu, K. Charge transfer from n-doped nanocrystals: Mimicking intermediate events in multielectron photocatalysis. *J. Am. Chem. Soc.* **2018**, *140*, 7791–7794. [CrossRef]
40. Lu, S.; Sui, L.; Liu, Y.; Yong, X.; Xiao, G.; Yuan, K.; Liu, Z.; Liu, B.; Zou, B.; Yang, B. White Photoluminescent Ti_3C_2 MXene Quantum Dots with Two-Photon Fluorescence. *Adv. Sci.* **2019**, *6*, 1801470. [CrossRef]
41. Wu, K.; Chen, J.; McBride, J.R.; Lian, T. Efficient hot-electron transfer by a plasmon-induced interfacial charge-transfer transition. *Science* **2015**, *349*, 632–635. [CrossRef]
42. Xie, Z.; Zhang, F.; Liang, Z.; Fan, T.; Li, Z.; Jiang, X.; Chen, H.; Li, J.; Zhang, H. Revealing of the ultrafast third-order nonlinear optical response and enabled photonic application in two-dimensional tin sulfide. *Photonics Res.* **2019**, *7*, 494–502. [CrossRef]
43. Wibmer, L.; Lages, S.; Unruh, T.; Guldi, D.M. Excitons and Trions in One-Photon- and Two-Photon-Excited MoS_2: A Study in Dispersions. *Adv. Mater.* **2018**, *30*, 1706702. [CrossRef]
44. Guo, J.; Shi, R.; Wang, R.; Wang, Y.; Zhang, F.; Wang, C.; Chen, H.; Ma, C.; Wang, Z.; Ge, Y.; et al. Graphdiyne-Polymer Nanocomposite as a Broadband and Robust Saturable Absorber for Ultrafast Photonics. *Laser Photonics Rev.* **2020**, *14*, 1900367–1900378. [CrossRef]
45. Breusing, M.; Ropers, C.; Elsaesser, T. Ultrafast Carrier Dynamics In Graphite. *Phys. Rev. Lett.* **2009**, *102*, 210–213. [CrossRef]
46. Kalanoor, B.S.; Bisht, P.B.; Ali, S.A.; Baby, T.T.; Ramaprabhu, S. Optical nonlinearity of silver-decorated graphene. *J. Opt. Soc. Am. B* **2012**, *29*, 669–675. [CrossRef]
47. Yu, Y.; Si, J.; Yan, L.; Li, M.; Hou, X. Enhanced nonlinear absorption and ultrafast carrier dynamics in graphene/gold nanoparticles nanocomposites. *Carbon* **2019**, *148*, 72–79. [CrossRef]